Journal of Solid State Chemistry 182 (2009) 2312–2318

Contents lists available at ScienceDirect

Journal of Solid State Chemistry

journal homepage: www.elsevier.com/locate/jssc

Order–disorder phase transformations in quaternary pyrochlore oxide system: Investigated by X-ray diffraction, transmission electron microscopy and Raman spectroscopic techniques

A.N. Radhakrishnan, P. Prabhakar Rao *, K.S. Sibi, M. Deepa, Peter Koshy

Materials and Minerals Division, National Institute for Interdisciplinary Science and Technology (NIIST), Trivandrum 695 019, India

ARTICLE INFO

Article history:
Received 18 December 2008
Received in revised form
3 June 2009
Accepted 6 June 2009
Available online 16 June 2009

Keywords:
Pyrochlore
Defect fluorite
Order–disorder transition
Raman spectra
TEM

ABSTRACT

Order–disorder transformations in a quaternary pyrochlore oxide system, Ca–Y–Zr–Ta–O, were studied by powder X-ray diffraction (XRD) method, transmission electron microscope (TEM) and FT-NIR Raman spectroscopic techniques. The solid solutions in different ratios, 4:1, 2:1, 1:1, 1:2, 1:4, 1:6, of $CaTaO_{3.5}$ and $YZrO_{3.5}$ were prepared by the conventional high temperature ceramic route. The XRD results and Rietveld analysis revealed that the crystal structure changed from an ordered pyrochlore structure to a disordered defect fluorite structure as the ratios of the solid solutions of $CaTaO_{3.5}$ and $YZrO_{3.5}$ were changed from 4:1 to 1:4. This structural transformation in the present system is attributed to the lowering of the average cation radius ratio, r_A/r_B as a result of progressive and simultaneous substitution of larger cation Ca^{2+} for Y^{3+} at *A* sites and smaller cation Ta^{5+} for Zr^{4+} at *B* sites. Raman spectroscopy and TEM analysis corroborated the XRD results.

1. Introduction

Pyrochlore oxides of the general formula, $A_2B_2O_7$ (*A* and *B* are metals) have considerable importance in both basic science [1–5] and engineering [6–9] and become a point of attraction for researchers, especially in material science. This is because pyrochlores lend themselves to a wide variety of substitution at the *A* and *B* sites provided the ionic radius ratio (r_A/r_B) and charge neutrality criteria are satisfied. The crystal structure can tolerate vacancies at *A* and *O* sites to an extent allowing cation and anion migration [10]. These compounds exhibit a wide variety of physical properties such as semiconducting properties, dielectric properties, ionic conductivity etc. [10]. Many vacancy containing pyrochlores possess good oxide ion conductivity and can be considered as a potential candidate as solid electrolytes for solid oxide fuel cell (SOFC) applications [11].

Ideal pyrochlore structure can be considered as an ordered defect fluorite structure with twice the lattice constant. Pyrochlore has a general formula $A_2B_2O_6O'$ where *A* is a bigger cation (~1 Å) and *B* is a smaller cation (~0.6 Å). Depending upon the oxidation state of *A* and *B* cation, oxide pyrochlores can be generally classified as $A_2^{3+}B_2^{4+}O_7$ (3+, 4+) and $A_2^{2+}B_2^{5+}O_7$ (2+, 5+) types. The existence, field of stability, synthesis and physical properties of (3+, 4+) and (2+, 5+) pyrochlores have discussed in detail by Subramanian et al. The *A* cation is eight coordinated and located within a distorted cubic polyhedron. The *B* cation is six coordinated and located within a distorted octahedron of oxygen. The O anions are coordinated to two *A* and two *B* cations whereas the O′ anion is tetrahedrally coordinated with only *A* cations. It belongs to the space group *Fd*3*m* (No. 227) with unit cell containing eight formula units. With the choice of the origin of the coordinate system at the *B* site, the atoms occupying the following crystallographically nonequivalent positions: *A* at 16*d*, *B* at 16*c*, O at 48*f* and O′ at 8*b* sites. A symmetrically equivalent 8*a* site is vacant. The 48*f* oxygen ions are characterized by a positional parameter, *x* and it depends on the choice of the origin. The lattice parameters are of the order of 10 Å and *x* parameter is found to vary from 0.3125 to 0.375 [10].

Ideal fluorite is a simple crystal structure having a general formula AO_2. The A^{4+} cation is eight coordinated with an fcc arrangement and O^{2-} anion occupying the tetrahedral holes within the cubic polyhedron. It belongs to the space group *Fm*3*m* (No. 225) and its unit cell contains four formula units. The atoms occupying the following special positions in the unit cell: A^{4+} cation at 4*a* and O^{2-} anion at 8*c* sites. The lattice parameter of the fluorite structure is ~5 Å and oxygen ion occupying a definite position with *x* parameter 0.375. But defect fluorite structure is anion deficient with a formula, $AO_{1.75}$ and one of the 8*c* sites is vacant [10].

The order–disorder transformation in a pyrochlore structure is of immense interest because this is the only oxide in which

* Corresponding author. Fax: +91 471 2491712.
E-mail address: padala_rao@yahoo.com (P. Prabhakar Rao).

0022-4596/$ - see front matter © 2009 Elsevier Inc. All rights reserved.
doi:10.1016/j.jssc.2009.06.016

order–disorder transformations occur in both the anion and cation arrangements. It has been reported earlier that disorder can be introduced into the structure by ion-irradiation [12–16], compositional changes (which lead to lower the difference in the ratio of the ionic size of the cations at the *A* sites to that at *B* sites) [11,17], pressure [18] and thermal treatment [19]. Disordered pyrochlore oxides are of great interest in the area of solid oxide electrolytes because they exhibit high oxide ion conductivity which makes them suitable for applications in SOFCs [17]. It is drawn from earlier investigations that one of the key parameters influencing structural disorder in $A_2B_2O_7$ pyrochlores is the cation radius ratio, r_A/r_B. As r_B approaches r_A, disorder in both the cations and anions sublattices increases ultimately resulting complete disorder characteristic of the defect fluorite structure as in the case of $Y_2(Ti_yZr_{1-y})_2O_7$ [20] and $Gd_2(Ti_yZr_{1-y})_2O_7$ when Zr content is high [21]. These types of disorder may lack stability of the phase for repeated thermal cycles. Apart from the cation ionic radius ratio (r_A/r_B) considerations, the investigations on $Y_2(Sn_xTi_{1-x})_2O_7$ and $Gd_2(Sn_xTi_{1-x})_2O_7$ solid solutions indicated that the crystal chemistry of *B* site cations (e.g. chemical bonding) have an important effect on the order–disorder transformation and the degree of disorder in the pyrochlore [22]. Recently, we reported new pyrochlore type oxides in a Ca–Y–Ti-Nb–O system which show some useful dielectric properties [23]. In the present investigation, we could prepare some quaternary pyrochlore type oxides in Ca–Y–Zr–Ta–O system in which pyrochlore (order) to defect fluorite (disorder) phase transformation is observed. This order–disorder phase transformation is studied by powder X-ray diffraction, Raman spectroscopy and transmission electron microscopy techniques. Some of these results are presented in this paper.

2. Experimental

Solid solutions in different stoichiometric compositions: $Ca_{1.6}Y_{0.4}Zr_{0.4}Ta_{1.6}O_7$, $Ca_{1.33}Y_{0.67}Zr_{0.67}Ta_{1.33}O_7$, $CaYZrTaO_7$, $Ca_{0.67}Y_{1.33}Zr_{1.33}Ta_{0.67}O_7$, $Ca_{0.4}Y_{1.6}Zr_{1.6}Ta_{0.4}O_7$ and $Ca_{0.29}Y_{1.71}Zr_{1.71}Ta_{0.29}O_7$ in a Ca–Y–Zr–Ta–O system were prepared by the conventional ceramic route using the starting materials, $CaCO_3$, Y_2O_3, ZrO_2 and Ta_2O_5 (ACROS ORGANICS, 99.99%). For better understanding, these compounds can be treated as different ratios of Ca–Ta–O and Y–Zr–O system that is 4:1, 2:1, 1:1, 1:2, 1:4, 1:6. These are represented as C4YZT4, C2YZT2, CYZT, CY2Z2T, CY4Z4T and CY6Z6T, respectively. (These nomenclatures are used in the later part of the text.) The raw materials were weighed according to the stoichiometry of the samples and then mixed thoroughly in an agate mortar. Acetone was added to the powdered mixture for proper mixing. Then, the mixture was dried in an air oven at 100 °C for 1 h. This procedure of mixing and subsequent drying was repeated thrice to get a homogeneous mixture. The powdered samples were calcined at 1300 °C for 6 h.

The calcined product was ground into a fine powder and then mixed with 2 wt% solution of polyvinyl alcohol (PVA) as the organic binder for strengthening and good compaction of the pellet. The dried powder was pressed into cylindrical pellets of 10 mm diameter and about 2–3 mm thickness using a hydraulic press. Pellets were initially heated to 600 °C and kept for 30 min to completely remove the organic binder and then sintered at a temperature of 1600 °C for 6 h. Powder X-ray diffraction patterns were recorded to identify the crystalline phase of the sintered samples using a Ni filtered Cu$K\alpha$ radiation by a Philip's X'pert Pro diffractometer operating at 40 kV and 30 mA. Scans were recorded over a 2θ range of 10–70° with a step size of 0.02° and a scan time per step 40 s using X'Pert software. The unit cell parameters were calculated by least square method and Rietveld analysis was also performed to refine the structure using X'pert plus software. The FT NIR Raman spectra of the powdered samples were recorded on a Bruker RFS100/S spectrometer using near infrared laser excitation (Nd: YAG, 1064 nm). Standard Ge detector cooled to liquid nitrogen temperature is used and it was set to scan over the range from 50 to 1000 cm^{-1}. The resolution of the spectrometer is 4 cm^{-1}. The selected area electron diffraction (SAED) pattern and high resolution electron microscopy (HREM) of the samples were carried out on a FEI TECNAI $30G^2$ S-TWIN transmission electron microscope (TEM) operating at 300 kV. The sintered samples were ground into very fine powder and a small amount of the powder is dispersed in acetone medium using ultrasonicator. The solution is drop casted on carbon coated copper grid using a micropipette and dried.

3. Results and discussion

3.1. Powder X-ray diffraction studies

Fig. 1 shows the powder XRD patterns obtained for various stoichiometric compositions: C4YZT4, C2YZT2, CYZT, CY2Z2T, CY4Z4T and CY6Z6T in the Ca–Y–Zr–Ta–O system. The XRD patterns of C4YZT4, C2YZT2, CYZT and CY2Z2T are similar to the earlier reported cubic pyrochlore type oxides of the formula $A_2B_2O_7$ such as $(Ca_{2/3}Y_{1/3})_2(Ti_{1/3}Nb_{2/3})_2O_7$ [23] and $Bi_{1.5}ZnNb_{1.5-x}Ta_xO_7$ [24]. All the reflections are indexed with respect to the cubic pyrochlore structure in the space group *Fd*3*m* (No. 227). The presence of super lattice reflections peaks like (111), (311), (331), (333), (531), (711) and (731) points to a doubling of the cubic-cell parameter, the characteristic peaks of the pyrochlore structure. It was further found that the intensity of the characteristic super-structure peaks diminishes on going from C4YZT4 to CY2Z2T as the $YZrO_{3.5}$ phase is increased. On the other hand, the absence of these pyrochlore characteristic peaks in the XRD patterns of CY4Z4T and CY6Z6T confirm the disorder of the cations at the *A* and *B* sites.

In general, the transformation from order to disorder in pyrochlore type oxides is attributed to the lowering of the ratio of the average ionic size at *A* site to that at *B* site (r_A/r_B). In the present system, this ratio varies from 1.69 to 1.46 as shown in Fig. 2 (the ionic radii of Ca^{2+} and Y^{3+}, in 8-fold coordination are 1.12 and 1.019 Å and that of Zr^{4+} and Ta^{5+} in 6-fold coordination are 0.72 and 0.64 Å, respectively). This structural transformation in the present system is attributed to the lowering of the average cation radius ratio, r_A/r_B as a result of progressive and simultaneous substitution of larger cation Ca^{2+} for Y^{3+} at *A* sites and smaller cation Ta^{5+} for Zr^{4+} at *B* sites. Usually, structural disorder takes place in pyrochlore type compounds as the average cation radius ratio (r_A/r_B) approaches unity. However, structural disorder induced in the present system (CY4Z4T) for $r_A/r_B = 1.47$ which is relatively higher than that observed in the transformation from the pyrochlore to the fluorite type phase in the $Ln_2Zr_2O_7$ system [25]. ($Y_2Zr_2O_7$ has a metastable pyrochlore structure having r_A/r_B, 1.42). Ordered pyrochlore is favoured when the radius ratio (r_A/r_B) of the cations lies within the range 1.46–1.78 (e.g. $La_2Zr_2O_7$, $r_A/r_B = 1.61$). Conversely, when the ratio is less than 1.46, a defect fluorite structure is favoured (e.g. $Y_2Zr_2O_7$, $r_A/r_B = 1.42$) [26]. Although, the r_A/r_B value controls the formation of pyrochlore structure and its transformation to a disordered fluorite state, however, no significant order–disorder structural transition occurs in the solid solution for which there is strong covalent bonding, e.g. in the systems of $Y_2(Sn_xTi_{1-x})_2O_7$ and $Gd_2(Sn_xTi_{1-x})_2O_7$ for the same range of r_A/r_B values in the $RE_2(Zr,Ti)_2$ solid solution. It is concluded from these results that other factors such as the crystal chemistry of *B* site cations (e.g.

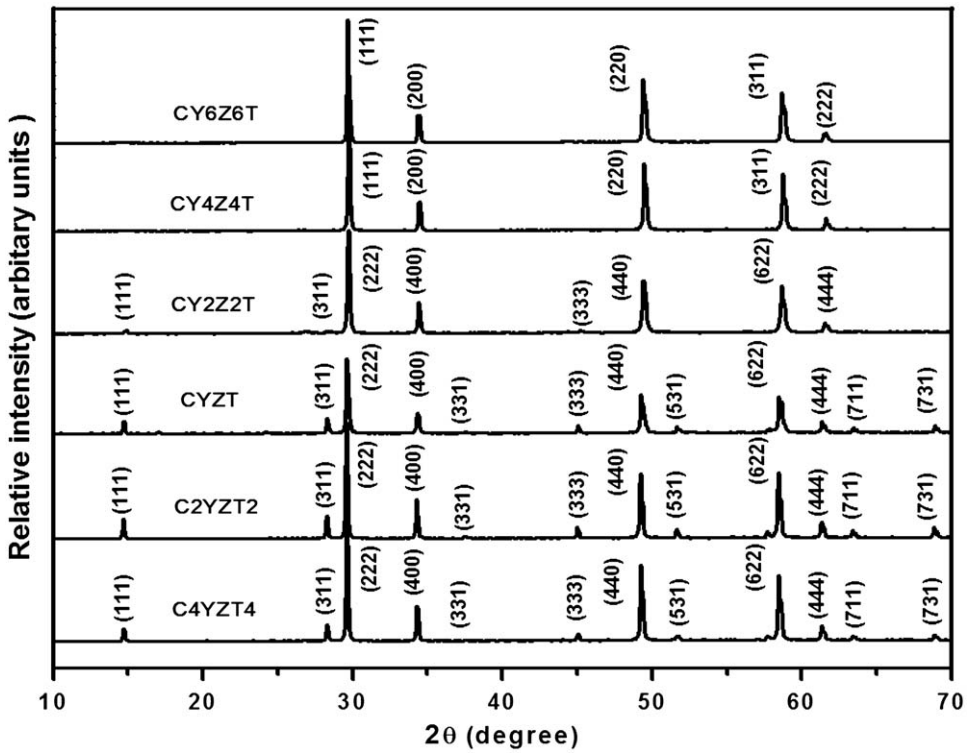

Fig. 1. Powder X-ray diffraction patterns for various compositions in the Ca–Y–Zr–Ta–O system.

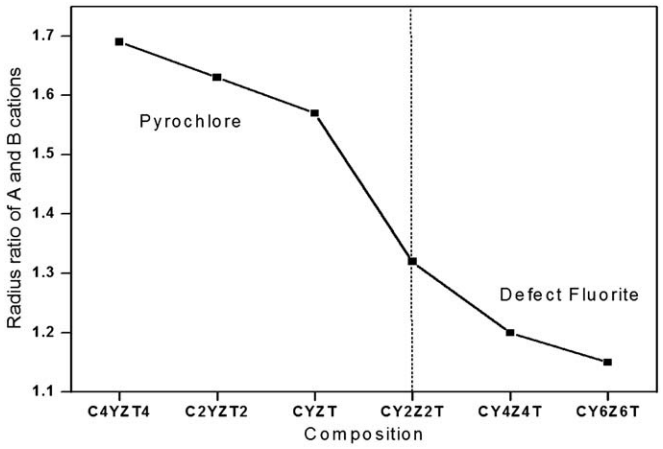

Fig. 2. Plot of radius ratio (r_A/r_B) as a function of various compositions in the Ca–Y–Zr–Ta–O system.

chemical bonding and the extent of covalency) have an important effect on the order–disorder transformation and the degree of disorder in the pyrochlore [22]. Therefore apart from cation radius ratio consideration, the structural transformation in the present system may be attributed to the crystal chemistry of the cations substituted at the *A* (Ca^{2+} for Y^{3+}) and *B* (Ta^{5+} for Zr^{4+}) sites.

The intensity ratios of superlattice peaks like (111), (311) and (331) with (222) reflection of the simulated ordered patterns and the observed patterns are compared in a plot (Fig. 3a). It should be mentioned here that for fully ordered XRD pattern of $Ca_2Ta_2O_7$ and $Y_2Zr_2O_7$, the super-structure peaks are very strong for $Ca_2Ta_2O_7$ due to large difference in scattering power of Ca and Ta, whereas the super-structure peaks are very tiny for fully ordered $Y_2Zr_2O_7$ presumably due to the fact that Y^{3+} and Zr^{4+} are isoelectronic. It is very clear from the plot that the peak intensity ratio values for the observed patterns are smaller than that of the simulated ordered patterns. This indicates that the decrease in peak intensity ratio values is not presumably contributed entirely due to the small scattering power difference of Y and Zr due to their isoelectronic nature. (The intensity ratios were calculated after normalizing to the maximum intensity peak and the XRD patterns were recorded for all the samples under identical measuring conditions). Therefore, the extent of structural disorder in the system is also contributing to the decrease in peak intensity ratios with increase of $YZrO_{3.5}$ content. To illustrate further, the ratios of the observed and calculated superlattice peaks of (111), (311) and (331) reflections (I_{obs}/I_{cal}) were plotted as a function of $YZrO_{3.5}$ content (Fig. 3b). As can be seen from the figure, the intensity ratios, I_{111}, I_{311} and I_{331}, are seen to be more or less same for the compositions, C4YZT4, C2YZT2, CYZT, and then decrease markedly at the phase boundary of pyrochlore and fluorite structure for the composition CY2Z2T, and finally the ratios become zero for CY4Z4T and CY6Z6T. Similar observations have been made in the study of the pyrochlore-fluorite phase transitions in $Ln_2Ti_2O_7$ ($Ln = Tm-Lu$) [27]. It has been observed that such structural disorder in pyrochlore type oxides displays remarkable change in ionic conductivity as in the case of $Gd_2(Ti_yZr_{1-y})_2O_7$ [21] and $Gd_{2-y}Nd_yZr_2O_7$ [28]. The increase in ionic conductivity is associated with cation antisite disorder which has been verified by XRD [29]. Furthermore, some pyrochlores undergo order–disorder transitions on substitutions of cations differing in valence state [30]. Here, in the present system, order–disorder transition is observed on going from Ca–Ta–O rich phase (Ca^{2+}/Ta^{5+} which have valence difference of 3) to Y–Zr–O rich phase (Y^{3+}/Zr^{4+} which have valence difference of 1). It also elucidates that the reduction in valence state between the cations occupying *A* and *B* sites might have contributed for the order–disorder phenomena observed in the present system in addition to the reasons cited above.

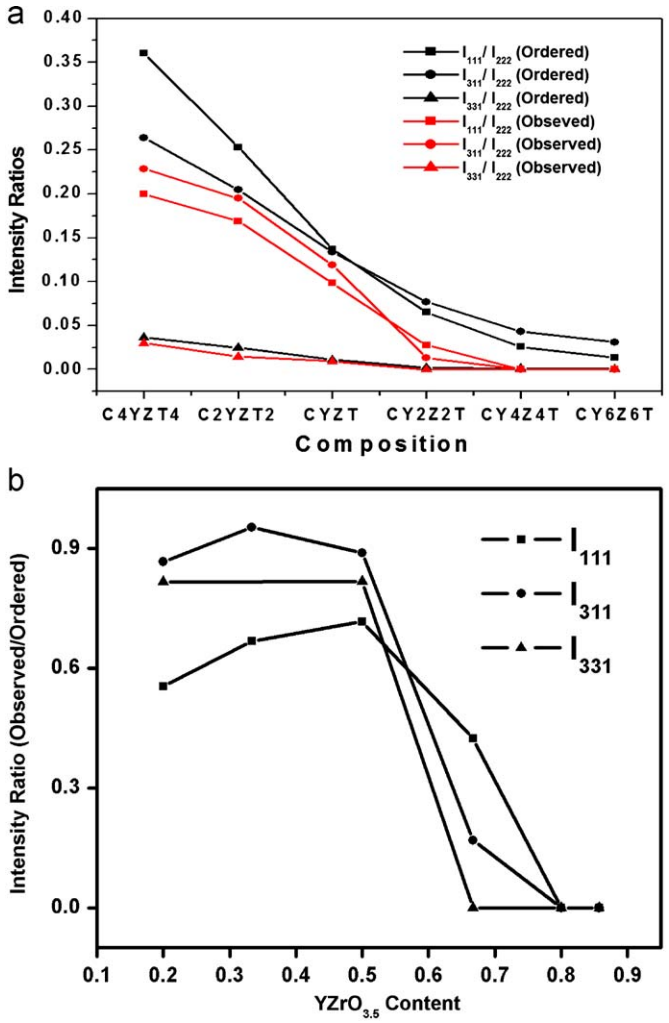

Fig. 3. (a) Comparison of intensity ratios (I_{111}/I_{222}, I_{311}/I_{222} and I_{331}/I_{222}) of simulated ordered XRD patterns and observed patterns for different compositions in the Ca–Y–Zr–Ta–O system. (b) I_{obs}/I_{cal} for (111), (311) and (331) reflections as a function of $YZrO_{3.5}$ content.

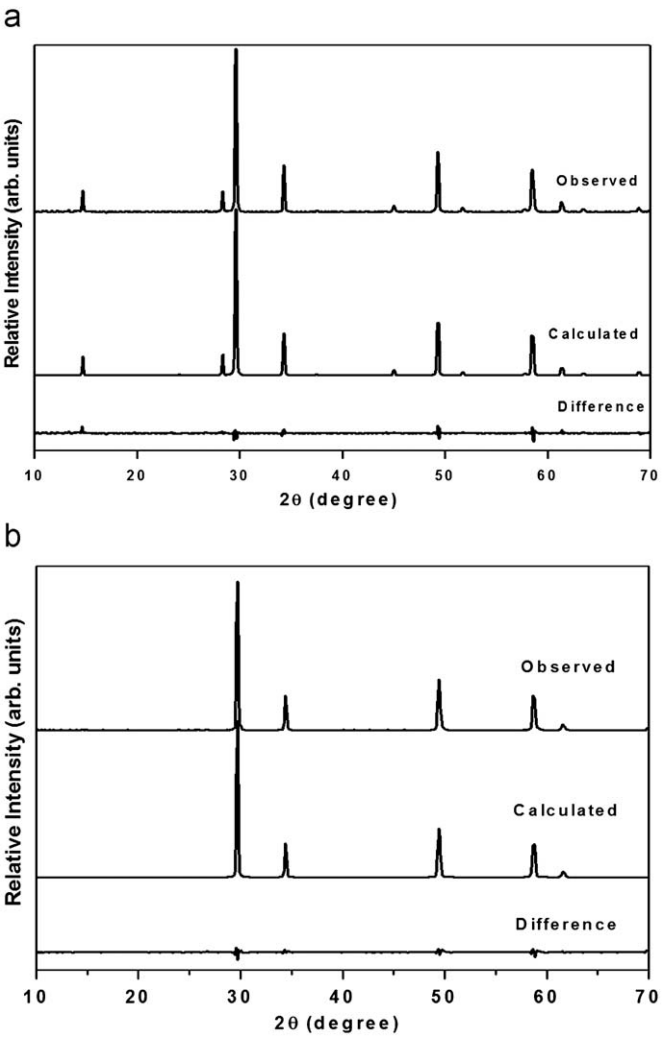

Fig. 4. Observed, calculated and difference XRD pattern profiles of (a) CYZT and (b) CY6Z6T.

Rietveld analysis of the XRD data of all the compositions in the Ca–Y–Zr–Ta–O system was carried out in the space group *Fd*3*m* (No. 227). The profile was fitted using pseudo-Voigt profile function. The refinement is in good agreement with the space group in all aspects, in which the *A* cations (A = Ca, Y) are at 16*d* sites ($\frac{1}{2},\frac{1}{2},\frac{1}{2}$) and the *B* ones ($B$ = Zr, Ta) at 16*c* (000). There are two types of oxygen: one at the 48*f* sites ($x,\frac{1}{8},\frac{1}{8}$) and the other at the 8*b* sites ($\frac{3}{8},\frac{3}{8},\frac{3}{8}$). The variable positional parameter (x) of the oxygen at 48*f* site determines the pyrochlore structure stability. Acceptable values for this oxygen coordinate are within the range 0.3125–0.375. The Rietveld analysis of the powder diffraction data of the samples C4YZT4, C2YZT2, and CYZT reveal that these three compositions belong to cubic pyrochlore system with space group *Fd*3*m* (No. 227). Fig. 4 shows observed, calculated and difference pattern of CYZT sample. The Rietveld refinement of CY2Z2T, CY4Z4T and CY6Z6T were performed by assuming the disordering of cationic and anionic sublattices to different extent. The *A* cation and *B* cation sites in pyrochlore become indistinguishable when it is transforming to a defect fluorite structure. The pyrochlore structure (space group *Fd*3*m*) was used as the starting model, assuming the intermixing of the cations at *A* and *B* sites. The cation disordering is due to antisite defect pair formation, accompanied by the generation of Frenkel defects in the anion sublattice which has a significant effect on the electrical properties of material [31]. As a result of this disordering, the intensity of superlattice peaks gets decreased, but still belong to space group *Fd*3*m* (No. 227). But in CY4Z4T and CY6Z6T cation disordering is maximum, led to structural transformation from pyrochlore to defect fluorite structure. Fig. 4 shows observed, calculated and difference pattern of CY6Z6T sample. Table 1 shows refined lattice parameters and *R*-values for various stoichiometric compositions. The lattice constant of the solid solutions increased linearly with the increasing of $CaTaO_{3.5}$ as expected based on the ionic size consideration of the cations.

Fig. 5 gives the variation of oxygen positional parameter, x as a function of different compositions. The structural stability of the compound is affected by the positional parameter (x) of the oxygen at *48f*. Considering an $A_2B_2O_7$ pyrochlore structure, varying this value changes the shape of the *A* and *B*-site polyhedra [32]. For a value of 0.375 for this fractional coordinate, the *A* and *B*-site polyhedra are regular cubes and trigonally flattened octahedra, respectively. When the x coordinate decreases to 0.3125, the *B*-site becomes a regular octahedron and the cubic *A*-site distorts into a trigonal scalenohedron. The deviation of oxygen at 48*f* from the special position ($x,\frac{1}{8},\frac{1}{8}$) with $x = 0.375$ is thus a sensitive measurement of the difference between a pyrochlore and a "defect fluorite" phase [10]. It has been observed after Rietveld analysis that with

Table 1
Refined lattice parameter and *R*-values for various compositions in the Ca–Y–Zr–-Ta–O system.

Composition	Crystal phase	Lattice constant (Å)	R_{exp} (%)	R_p (%)	R_{wp} (%)	GOF
CY6Z6T	Defect fluorite	10.4326(7)	5.06	6.61	9.97	3.87
CY4Z4T	Defect fluorite	10.4364(6)	11.95	11.26	17.28	2.09
CY2Z2T	Pyrochlore	10.444(1)	9.83	13.77	18.62	3.58
CYZT	Pyrochlore	10.4652(8)	11.16	11.46	17.26	2.39
C2YZT2	Pyrochlore	10.4725(6)	9.78	14.20	17.53	3.21
C4YZT4	Pyrochlore	10.4730(5)	10.62	15.95	20.00	3.55

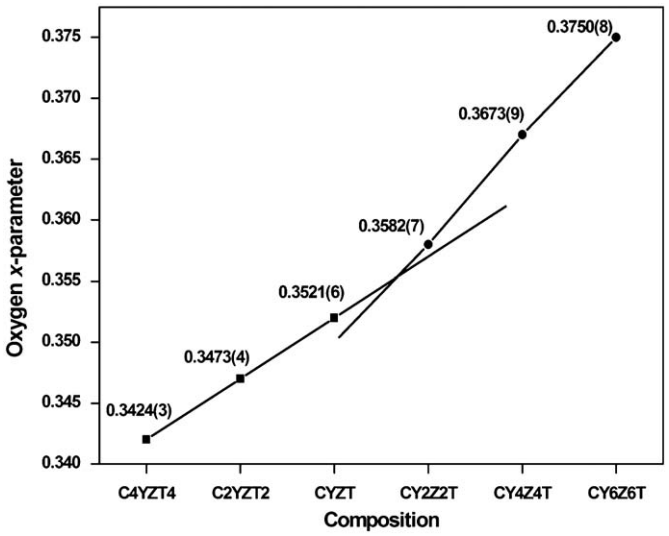

Fig. 5. Variation of oxygen *x*-parameter as a function of different compositions in the Ca–Y–Zr–Ta–O system.

increase of $YZrO_{3.5}$ phase in the system, the positional parameter, *x* increases which in turn drives the system to transform from ordered pyrochlore to disordered pyrochlore and finally to defect fluorite.

3.2. Raman spectroscopic studies

Raman spectroscopic investigation provides information to distinguish between a defect-fluorite structure and the pyrochlore structure [33]. Based on the crystal structure and group theory analysis, there are only six Raman active modes for the pyrochlore structure.

$$\Gamma_{\text{raman}} = A_{1g} + E_g + 4F_{2g}$$

A and *B* cations do not contribute to Raman active vibrations since they are located at the inversion centre and the six Raman active modes involve only the movement of oxygen atoms. One of the F_{2g} modes is caused by the 8*a* oxygen sub-lattice vibration and other modes are attributed to 48*f* oxygen sub-lattice vibrations. For ideal fluorite structure there is only one F_{2g} mode related to 8*c* site [34]. From experimental data, defect fluorite structure normally has weak Raman peaks [33]. More Raman lines other than theoretically calculated, may appear in the Raman spectra of pyrochlores and fluorites due to various reasons as discussed by Glerup et al. [34].

The FT Raman spectra for different stoichiometries in Ca–Y–Zr–Ta–O system are shown in Fig. 6. The Raman bands are broad as compared to that of well ordered crystalline compounds,

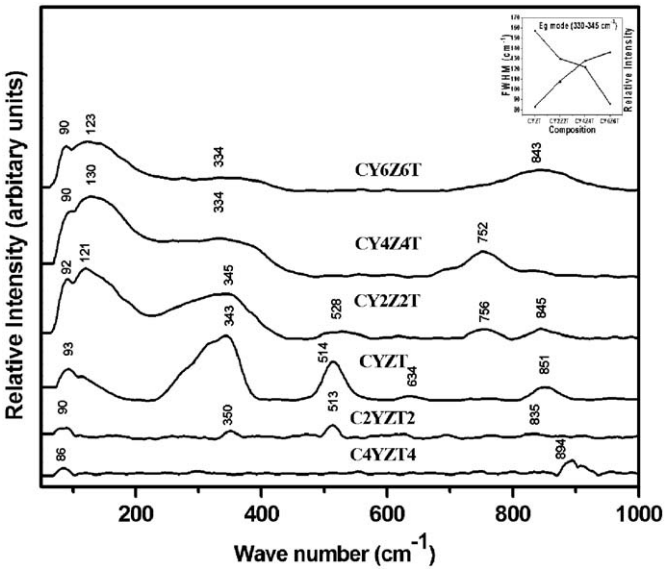

Fig. 6. FT NIR Raman spectra of the samples sintered at 1600 °C for 6 h. The inset shows variation of FWHM and intensity of the vibrational mode, E_g as a function of different compositions.

similar to that observed by Scheetz et al. for pyrochlore zirconates [35]. The Raman spectra of CYZT shows major Raman modes of pyrochlores like A_{1g} at 514 cm^{-1}, E_g at 343 cm^{-1} and one F_{2g} band at 634 cm^{-1} with considerable intensity [36]. Other F_{2g} modes are too weak to be observable and additional peaks appeared around 100 and 850 cm^{-1} may be due to local lattice modes arising due to distortion of the octahedra [37]. But it is very difficult to take the Raman spectra of C4YZT4 and C2YZT2 samples because of their high fluorescence and as a result, the relative intensity of Raman peaks became very less or indistinguishable from the noise. Also it is already reported that as the content of Ta is increased at *B* site in $A_2B_2O_7$ pyrochlores, intensity of the Raman lines becomes weaker and weaker [34]. Raman spectrum of CY2Z2T is almost similar to that of CYZT, but the intensity of the peaks became very low and peaks corresponding to local disordering become relatively intense. Small distortions of the atomic positions caused by *B* cation species in pyrochlore structure compounds affect the force constant of vibrational mode resulting small shift in vibrational frequency. Thus, the full width at half maximum (FWHM) of a vibrational mode provides a measure of the level of localized short range structural disorder in the materials [32]. Typically, the FWHM of the vibrational mode, E_g (330–345 cm^{-1}), increases considerably with changing slope in the phase boundary combined with the decrease of Raman intensity for the progressive and simultaneous substitution of larger cation Ca^{2+} for Y^{3+} at *A* sites and smaller cation Ta^{5+} for Zr^{4+} at *B* sites (shown as inset in Fig. 6). This clearly confirms that pyrochlore structure is getting disordered as revealed through XRD analysis. Raman spectra of CY4Z4T and CY6Z6T show considerable difference from that of other samples and the broadening of the Raman bands is due to structural disorder [33]. Raman peaks corresponding to A_{1g}, and E_g of pyrochlore becomes very less in intensity whereas peaks corresponding to local lattice modes become comparably intense. However, the F_{2g} mode usually observed at ~466 cm^{-1} for ideal fluorite structured oxides ThO_2, CeO_2, etc., was not observed by us [33]. The extra bands observed around 760 cm^{-1} for CY4Z4T and 840 cm^{-1} for CY6Z6T can be attributed to seven coordinated *A* cation in the defect fluorite structure [36,37]. Therefore the structural transformation from ordered pyrochlore phase to more disordered fluorite phase can be confirmed from the Raman spectra.

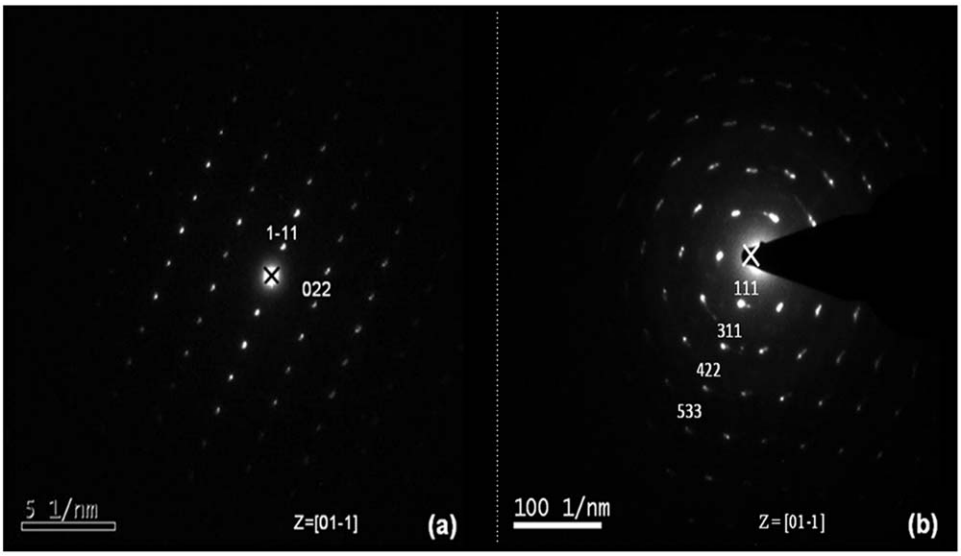

Fig. 7. Selected Area Electron Diffraction (SAED) patterns of (a) C2YZT2 and (b) CY6Z6T.

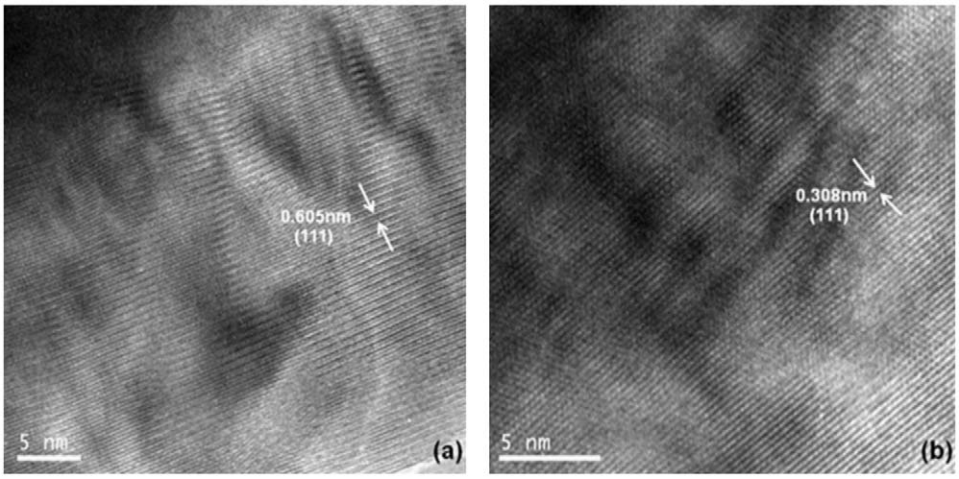

Fig. 8. High resolution TEM images of (a) CYZT and (b) CY6Z6T.

3.3. TEM studies

Fig. 7 shows the selected area electron diffraction patterns (SAED) recorded from C2YZT2 and CY6Z6T samples which can be indexed according to a pyrochlore unit cell and fluorite type unit cell, respectively. SAED pattern of C2YZT2 shows highly ordered diffraction maxima with the appearance of weak superlattice diffraction spots in between the bright diffraction spots. The absence of weak super lattice diffraction spots in CY6Z6T SAED pattern distinguishes from the pyrochlore unit cell and the diffraction maxima arranged in a ring pattern is similar to that observed in a fluorite type SAED pattern of $Ce_2Zr_2O_7$ [16]. High resolution TEM images of CYZT and CY6Z6T are also shown in Fig. 8. The lattice constant of the fluorite structure layer is one half that of the pyrochlore unit cell layer as shown by the difference of the (111) spacing (Fig. 8). These results are in support of the XRD.

4. Conclusion

In summary, the present study determined the structural variation, Pyrochlore to Fluorite type in the solid solutions of different ratios: 4:1, 2:1, 1:1, 1:2, 1:4, 1:6 of $CaTaO_{3.5}$ and $YZrTaO_{3.5}$. The pyrochlore phase stabilizes for the r_A/r_B 1.69–1.57 and the defect fluorite phase for 1.47–1.45 values. The structural disorder induced in the present system for $r_A/r_B = 1.47$ as the ratios of the solid solutions of $CaTaO_{3.5}$ and $YZrTaO_{3.5}$ were changed from 4:1 to 1:4. This ratio, r_A/r_B is much higher than that observed in the transformation from the pyrochlore-type to the fluorite-type phase in the $Ln_2Zr_2O_7$ system. Therefore apart from cation radius ratio consideration, the structural transformation in the present system may be attributed to the crystal chemistry of the cations substituted at the *A* (Ca^{2+} for Y^{3+}) and *B* (Ta^{5+} for Zr^{4+}) sites.

Acknowledgments

One of the authors, A.N. Radhakrishnan, would like to acknowledge Council of Scientific Industrial Research (CSIR), Govt. of India, for the financial support towards junior research fellowship.

References

[1] M.A. Subramanian, A.P. Ramirez, G.H. Kwei, Solid State Ionics 108 (1998) 185–191.
[2] A.J. Garcia-Adeva, D.L. Huber, Phys. B 320 (1–4) (2002) 18–22.
[3] J.S. Gardner, B.D. Gaulin, S.H. Lee, C. Broholm, N.P. Raju, J.E. Greedan, Phys. Rev. Lett. 83 (1) (1999) 211–214.
[4] A.K. Hassan, L.P. Lévy, C. Darie, P. Strobel, Phys. Rev. B 67 (2003) 214432.
[5] J.D.M. Champion, A.S. Wills, T. Fennell, S.T. Bramwell, J.S. Gardner, M.A. Green, Phys. Rev. B 64 (2001) 140407.
[6] J. Lian, X.T. Zu, K.V.G. Kutty, J. Chen, L.M. Wang, R.C. Ewing, Phys. Rev. B 66 (2002) 054108.
[7] B.D. Begg, N.J. Hess, W.J. Weber, R. Devanathan, J.P. Icenhouer, S. Thevuthasan, B.P. McGrail, J. Nucl. Mater. 288 (2001) 208–216.
[8] S. Lutique, D. Staicu, R.J.M. Konings, V.V. Roudinella, J. Somers, T. Wiss, J. Nucl. Mater. 319 (2003) 59–64.
[9] S. Lutique, R.J.M. Konings, V.V. Rondinella, J. Somers, T. Wiss, J. Alloys Compd. 352 (2003) 1–5.
[10] M.A. Subramanian, G. Aravamudan, G.V. Subba Rao, Prog. Solid State Chem. 15 (1983) 55–143.
[11] P.K. Moon, H.L. Tuller, Solid State Ionics 28 (1988) 470.
[12] N.J. Hess, B.D. Begg, S.D. Conradson, D.E. McCready, P.L. Gassman, W.J. Weber, J. Phys. Chem. B 106 (2002) 4663–4677.
[13] J. Lian, L.M. Wang, S.X. Wang, J. Chen, L.A. Boatner, R.C. Ewing, Phys. Rev. Lett. 87 (2001) 145901.
[14] L. Lian, L. Wang, J. Chen, K. Sun, R.C. Ewing, J. Matt Farmer, L.A. Boatner, Acta Mater. 51 (2003) 1493–1502.
[15] S.X. Wang, L.M. Wang, R.C. Ewing, G.S. Was, G.R. Lumpkin, Nucl. Instrum. Methods B 148 (1999) 704–709.
[16] J. Lian, L.M. Wang, R.G. Haireb, K.B. Helean, R.C. Ewing, Nucl. Instrum. Methods B 218 (2004) 236–243.
[17] B.J. Wuensch, K.W. Eberman, C. Heremans, E.M. Ku, P. Onnerud, E.M.E. Yeo, S.M. Haile, J.K. Stalick, J.D. Jorgensen, Solid State Ionics 129 (2000) 111–133.
[18] F.X. Zhang, B. Manoun, S.K. Saxena, Mater. Lett. 60 (2006) 2773–2776.
[19] B.J. Wuensch, K.W. Eberman, JOM J. Miner. Met. Mater. Soc. 52 (2000) 19.
[20] Y. Liu, R.L. Withers, L. Noren, J. Solid State Chem. 177 (2004) 4404–4412.
[21] P.K. Moon, H.L. Tuller, Solid State Ionics 28–30 (1988) 470–474.
[22] R.C. Ewing, W.J. Weber, J. Lian, J. Apply. Phys. 95 (2004) 5949–5971.
[23] K. Ravindran Nair, P. Prabhakar Rao, A.V. Raj, S.K. Joseph, M.R. Chandran, P. Koshy, J. Am. Ceram. Soc. 90 (2007) 3656–3659.
[24] Q. Wang, H. Wang, X. Yao, J. Appl. Phys. 101 (2007) 104116.
[25] H. Yamamura, N. Nishino, K. Kakinuma, N. Nomura, Solid State Ionics 158 (2003) 359–365.
[26] K.R. Whittle, L.M.D. Cranswick, S.A.T. Redfern, I.P. Swainson, G.R. Lumpkin, J. Solid State Chem. 182 (2009) 442–450.
[27] A.V. Shlyakhtina, A.V. Knotko, M.V. Boguslavskii, S.Yu. Stefanovich, D.V. Peryshkov, I.V. Kolbanev, L.G. Shcherbakova, Solid State Ionics 176 (2005) 2297–2304.
[28] B.P. Mandal, S.K. Deshpande, A.K. Tyagi, J. Mater. Res. 23 (2008) 911.
[29] P.K. Moon, H.L. Tuller, in: G. Nazri, R.A. Huggins, D.F. Shriver (Eds.), Solid State Ionics Proceedings Symposium, vol. 135, Materials Research Society, Pittsburgh, 1990, p. 149.
[30] A.V. Shlyakhtina, O.K. Karyagina, L.G. Shcherbakova, Inorganic Mater. 40 (2004) 67–74.
[31] W.R. Panero, L. Stixrude, Phys. Rev. B 70 (2004) 054110–054111.
[32] B.P. Mandal, A. Banerjee, V. Sathe, S.K. Deb, A.K. Tyagi, 180 (2007) 2643–2648.
[33] B.P. Mandal, N. Garg, S.M. Sharma, A.K. Tyagi, J. Solid State Chem. 179 (2006) 1990–1994.
[34] M. Glerup, O. Faurskov Nielsen, F. Willy Poulsen, J. Solid State Chem. 160 (2001) 25–32.
[35] B.E. Scheetz, W.B. White, J. Am. Ceram. Soc. 62 (1979) 468–470.
[36] H.C. Gupta, S. Brown, N. Rani, V.B. Gohel, Int. J. Inorg. Mater. 3 (2001) 983–986.
[37] D. Huiling, Y. Xi, J. Mater. Sci. Mater. Electron. 15 (2004) 613–616.